Where and how the East Madagascar Current retroflection originates ?

Juliano D. Ramanantsoa[1,2,10] *, P. Penven[3], R. P. Raj[4], L. Renault[5], L. Ponsoni[6], M. Ostrowski[7], A. F. Dilmahamod[8,9], M. Rouault[1,2]

[1]Department of Oceanography, University of Cape Town (UCT), South Africa
[2]Nansen Tutu for Marine Environmental Research, Ma-Re Institute, University of Cape Town (UCT), South Africa
[3]Univ. Brest, CNRS, IRD, Ifremer, Laboratoire d'Océanographie Physique et Spatiale (LOPS), IUEM, Brest, France
[4]Nansen Environmental and Remote Sensing Center (NERSC), Bjerknes Center for Climate Research (BCCR), Bergen, Norway
[5]Department of Atmospheric and Oceanic Sciences, University of California, Los Angeles, Los Angeles, California, and Laboratoire d'Étude en Geophysique et Océanographie Spatiale, IRD, Toulouse, France
[6]Georges Lemaître Centre for Earth and Climate Research (TECLIM), Earth and Life Institute, Université catholique de Louvain, Louvain-la-Neuve, Belgium
[7]Institute of Marine Research (IMR), Bergen, Norway
[8]GEOMAR Helmholtz Centre for Ocean Research Kiel, Kiel, Germany
[9]Department of Oceanography, Dalhousie University, Halifax, Nova Scotia B3H 4R2, Canada
[10]Institut Halieutique et des Sciences Marines (IH.SM), Toliara, Madagascar

Key Points:

- The East Madagascar Current (EMC) retroflection is assessed.
- Evidence of Early Retroflection is demonstrated for the first time.
- Retroflection regimes are associated with EMC strength and eddy activity.
- Knowledge of EMC retroflection state helps understanding regional ecosystems variability.

*Department of Oceanography, University of Cape Town, office 123, Private Bag X3, Rondebosch 7701, Cape Town, South Africa

Corresponding author: Juliano Heriniaina Dani Ramanantsoa, `oceanman1@live.fr`

Abstract

In-situ and remote sensing data are used to identify three states of the East Madagascar Current (EMC) southern extension : Early-Retroflection, Canonical-Retroflection and No-Retroflection. Retroflections occur 47% of the time. EMC strength regulates the retroflection state, although impinged mesoscale eddies also contribute to the retroflection formation. The Early-Retroflection is linked with the EMC volume transport. Anticyclonic eddies drifting from the central Indian Ocean to the coast favors Early-Retroflection formation, anticyclonic eddies near the southern tip of Madagascar promotes the generation of Canonical Retroflection, and No-Retroflection appears to be associated with a lower Eddy Kinetic Energy (EKE). Knowledge of the EMC retroflection state could help predicting : (1) coastal upwelling south of Madagascar, (2) the South-East Madagascar phytoplankton bloom, (3) the formation of South Indian Ocean Counter Current (SICC). The EMC retroflection status appears to have a slight noticeable impact on the Agulhas Current system.

Plain Language Summary

The Indian Ocean (IO) is the fastest warming ocean in the world for the last two decades. Western boundary currents in this ocean, such as the East Madagascar Current (EMC), play a key role in transporting heat from the tropics toward the poles. There is a crucial need to assess the functioning of the EMC. This study found that the EMC retransports back through a retroflection 47% of water mass toward the IO instead of flowing mainly toward the pole. The retroflection occurs in different characteristics : an abrupt retroflection from the east coast of Madagascar is defined as an Early-Retroflection, Canonical-Retroflection occurs at the south-west of the island, and No-Retroflection attributed to the flow approaching the African coastline and flowing straight to the Agulhas Current (AC). Variation of EMC surface speed and the contribution of mesoscale eddy activity are associated with the retroflections generation. EMC retroflection occurrence has an impact on the coastal upwelling, prevalence of the South-East phytoplankton bloom, formation of the SICC, as well as influencing the AC variability. Based on climate change scenarii, the intensification of the EMC and multiple arrival of eddies may generate more EMC Early-Retroflection which may induce an imbalance in the IO recirculation.

1 Introduction

The East Madagascar Current (EMC), a western boundary current flowing poleward along the east coast Madagascar, constitutes a major contributor of the Agulhas Current (AC) system (*Lutjeharms et al.*, 1981; *Penven et al.*, 2006). Before propagating towards the AC, the EMC southern extension is also perceived to drift eastward towards western Australia and to act as a feeder of the South Indian Ocean Countercurrent (SICC) (*Lutjeharms*, 1988; *Siedler et al.*, 2006; *Palastanga et al.*, 2006). *Siedler et al.* (2009) elucidated the existence of a non-permanent EMC southern extension retroflection with a significant proportion going straight toward the AC and almost the half of it propagating into the SICC.

The EMC retroflection is also supposed to transport nutrient-rich waters, favouring phytoplankton blooms in the Madagascar basin (*Longhurst*, 2001; *Raj et al.*, 2010; *Dilmahamod et al.*, 2019). The presence of the EMC southern extension is also known to influence coastal upwelling at the southern tip of Madagascar (*Ramanantsoa et al.*, 2018a; *Ramanantsoa*, 2018b) with implications for local biological productivity (*Bemiasa*, 2009).

Nevertheless, very few studies have addressed the EMC southern extension, resulting in the lack of an exact definition of the EMC retroflection concept. There is a crucial need to understand the exact origin, occurrence, functioning, as well as the consequences of the EMC retroflection. Here, using a suite of Vessel-Mounted Acoustic Doppler Current Profiler (VMADCP) measurements, recorded current meter long-term observation, surface drifter data, as well as altimeter-derived sea level height, we show the characteristics of EMC retroflection, and we determine the associated dynamical processes, as well as the local and regional impacts.

2 Data and Methods

A compilation of VMADCP measurements is collected during five different research cruises operated around the EMC retroflection region. Explicit details of cruise data are given in the supporting information (Table S1). VMADCP data are used to highlight the structure of the EMC at 25°S.

A 2.5 years (10/2010 to 02/2013) time series of EMC volume transport (*Ponsoni et al.*, 2016) from a combination of several mounted Acoustic Doppler Current Profiler (ADCPs) and Recording Current Meters (RCMs) deployed at 23°S is used to measure the link between the daily volume transport of the EMC and the characteristics of its associated retroflection.

All available surface drifters trajectories passing in the EMC region are collected from the Global Drifter Programme database (`http://www.aoml.noaa.gov/envids/gld/krig/parttrk_id_temporal.php`).

Satellite altimetry sea surface height, distributed by the Copernicus Marine and Environment Monitoring Service (CMEMS) (`http://marine.copernicus.eu/services-portfolio/access-to-products/`), is used to derive geostrophic velocity of EMC and to detect the retroflection spatial extent for the period of 1993 to 2017.

The EMC retroflection is identified from altimetry by selecting a specific sea level height contour as a streamline representative of the EMC path. This methodology is equivalent to the one applied for the AC by *Backeberg et al.* (2012); *Loveday et al.* (2014); *Renault et al.* (2017). The selected contour is chosen as the mean sea level in the EMC southern extension region (42°E to 50°E and 22°S to 28°S), over a bathymetry ranging from 200 m to 2000 m, and with geostropic current speeds higher than 35 cm s^{-1}. The westernmost contour position determines the EMC retroflection location.

Monthly AC retroflection positions are also tracked using a similar method to assess the sensitivity of AC system in response to the EMC retroflection events.

3 Results

3.1 Contrasted behaviour of the EMC Southern extension from in-situ observations

VMADCP data reveal the horizontal structure of the EMC, characterised by a narrow poleward jet (∼175 km), close to the shelf break around ∼25°S, with an averaged core's velocity of 45 cm s^{-1} (Figure 1a-e (top)). On the eastern side of the EMC (25°S), an opposite flow is observed, ∼175 km from the coast, with an average velocity of 40 cm s^{-1} (Figure 1a-e (top)), consistent with *Nauw et al.* (2008).

All sections present opposite meridional velocities between the EMC and the return flow (Figure 1a-e (bottom)). However, while the EMC meridional velocity is consistently intense beyond ∼250 m depth, the return flow starts to weaken below 100 m depths (Figure 1a-e (bottom)). The presence of such opposing currents with almost similar ve-

119 locities may suggest a rotating flow (*Halo et al.*, 2014). Small difference in surface ve-
120 locities and significant differences in meridional velocities at depth could be indicative
121 of eddy-mean flow interactions when anticyclonic eddies shallower than the EMC approach
122 the Madagascan coast near 24°S. Eddy-EMC interactions may induce a transfer of mo-
123 mentum toward the mean flow (*Halo et al.*, 2014). *Nauw et al.* (2006) also reported an
124 anticyclonic shear close to the core of EMC in the observed vertical transect from VMADCP
125 at 25°S (see their Figure 5a).

126 To obtain a broader view of the circulation, altimeter sea surface height is over-
127 layed on top of VMADCP surface velocities. A good agreement is found between the two
128 products (Figure 1b-e). Figure 1b-e shows evidences of anticyclonic eddies drifting bet-
129 ween latitude of 22°S and 24°S from the Indian Ocean to the Madagascar coastline, in
130 agreement with previous reports (*Quartly et al.*, 2006). The anticyclonic eddies appear
131 to merge with the EMC mostly around 25°S.

132 A larger scale view of sea level height is illustrated on Figure 1g-j. The retroflec-
133 tion positions are identified during the same period of the collected VMADCP and are
134 detected in three different locations : Figure 1g and Figure 1i detect retroflection fur-
135 ther down in the AC region which is indicative of no EMC retroflection, while Figure 1h
136 and Figure 1j show retroflection at the southern extension of EMC. Interestingly, while
137 Figure 1h reveals a retroflection beyond the southern tip of Madagascar, Figure 1j shows
138 the presence of a retroflection prematurely formed along the southeast coast of the is-
139 land.

140 ### 3.2 Three states of retroflection extent

141 Global drifter data are used to assess the presence of retroflections in the EMC sou-
142 thern extension. Figures 2a,b,c depict trajectories of drifters showing the EMC retroflec-
143 tion paths. 19 drifters are counted to passively follow the early detachment of EMC, while
144 11 drifters trajectories are captured to follow the retroflection around the southern tip
145 of the island. In the case of no retroflection, 18 long-life drifters are found to join directly
146 the AC. Drifters travel time is given in each drifter trajectory. On average, the drifters
147 take six months to one year to pass through the EMC (Figure 2a in red dotted box) un-
148 til being advected beyond 60°E for a sudden eastward drift near 25°S (Figure 2a). Ho-
149 wever, drifters representing the retroflection further south take more time, about one-
150 year and a half. Drifters travel two to three years to delineate the early-gyre in the sou-
151 thwest south Indian Ocean (Figure 2c). Selection technique and a list of drifters are sum-
152 marised on Figure S2 and Table S2.

153 Monthly EMC retroflection positions are detected from satellite altimetry product
154 for 1993 to 2017. Figures 2d,e,f show the mean position of the EMC retroflections illus-
155 trated by red stars. Figure 2g highlights the spatial distribution of EMC retroflections.
156 They are partitioned using the statistic unsupervised k-mean clustering method (Text
157 S1), assuming the existence of three classes. Each classified retroflection positions are
158 combined to build, according to retroflection types, the mean positions composite men-
159 tioned in Figures 2d,e,f. The three distinct cases of EMC retroflection obtained are : Early-
160 Retroflection, Canonical-Retroflection, and No-Retroflection. Both drifter trajectories
161 (Figures 2a,b,c) and satellite data (Figures 2d,e,f) confirm the presence of EMC retro-
162 flection case scenarios. On monthly timescales during the period of 1993 to 2017, an EMC
163 retroflection is identified over 47% of events (Early Retroflection : 13% ; EMC Canoni-
164 cal Retroflection : 34%). The 53% remaining correspond to the case when the flow does
165 not retroflect and reach the African coastline to propagate straight into the Agulhas sys-
166 tem. This is in line with the findings of *Siedler et al.* (2009) with the addition of the Early-
167 Retroflection case as a new state of the EMC.

168 The EMC Early-Retroflection is the sudden eastward drift of EMC from the east
169 coast of Madagascar. The highest longitudinal probability of the Early Retroflection po-

sition is at 47.6°E±0.41, while it is at 43.8°E±1.8 for the Canonical Retroflection (Figure 2h). Early-Retroflection latitudinal average positioning is 25.65°S (Figure 2i).

3.3 Description of Early Retroflection events

This section aims (1) to confirm the presence of Early-Retroflection according to the EMC volume transport, and (2) to define the characteristics and implication of an Early-Retroflection.

Here, to address the drivers of Early-Retroflection events, we use an integrated EMC volume transport time series collected from long-term observation of ADCPs and RMCs combined data sets (*Ponsoni et al.*, 2016). In addition, an EMC altimeter-based geostrophic velocity is retrieved from the nearest location of the moored ADCPs point to the mid-transect. A significant linear relationship, coefficient correlation factor of 0.6, is found between the two time series on daily time scales (Figure 3a,b).

The EMC Early-Retroflection position is tracked on a daily frequency during the ADCP data period. Results reveal that occurrences of Early-Retroflections coincide with more intense EMC volume transports (Figure 3a,c). During the time-period of 11/10/2010 to 01/04/2013, Early-Retroflections on average occur 15 days a month. An Early-Retroflection is also found to persist over two months (12/2010 to 01/2011) when the volume transport of EMC reached 45 Sverdrup, while it did not occur for three consecutive months (03/2012 to 05/2012) when the transport was around 18 Sverdrup (*Ponsoni et al.*, 2016; *Ramanantsoa*, 2018b)). Weak volume transports are not associated with high frequencies of Early-Retroflection.

A selection of intense volume transport periods (data above one standard deviation) are used to construct a composite maps of sea level height and ocean colour. Figure 3d and Figure 3e present typical characteristics of an Early-Retroflection at 24.5°S. This link between larger transports and Earlier Retroflections is in agreement with previous theoretical work applied for the Agulhas Retroflection (*Ou and De Ruijter*, 1986). Figure 3d shows that the Early-Retroflection appears to originate from 24.5°S (black star) and drift following an eastward zonal band at ∼26°S. A high value of sea level is observed in that position, indicative of an anticyclonic rotation, which seems to be responsible for the rapid eastward drift at this latitude. This is confirmed by Figure 3f which depicts intense and wide positive vorticity, indicative of anticyclonic eddies along the east coast. Mesoscale anticyclonic eddies are known to drift from offshore and propagate into the EMC (*de Ruijter et al.*, 2004; *Dilmahamod et al.*, 2019). Consequently, the arrival of anticyclonic eddies increases the strength of the EMC and induces an abrupt detachment of the flow from the coast. In summary, the intense volume transport of the EMC (Figure 3a) together with the contribution of mesoscale eddies promotes Early-Retroflection occurrences (Figure 3c). In addition, the early detachment of the EMC presents also a signature in chlorophyll-a extending from the upwelling cell south of Madagascar (*Ramanantsoa et al.*, 2018a) to more than 2° in Longitude offshore (Figure 3e). Such offshore transport of coastal material illustrates how EMC Early Retroflections in the EMC could favour the presence of phytoplankton blooms in the Madagascar basin (*Dilmahamod et al.*, 2019).

3.4 Dynamical processes

Figure 4a presents the occurrences of retroflection cases (red and blue colours), the EMC surface geostrophic velocity anomalies and the surface Eddy Kinetic Energy (EKE; for the East and West Madagascar boxes shown on Figure 4b and 4c) for the period 1993 to 2017. Figures 4e,f,g reveal the structures of EMC southern extension computed as composites associated with values of EMC surface current anomalies and EKE variations shown on Figure 4a.

Figure 4e shows the ADT composite associated with anomalous high EMC surface speeds (above one standard deviation) and anomalous high EKE (above one standard deviation in the green box in Figure 4b). In agreement with the previous section, it corresponds to an Early-Retroflection. Positive abnormal high EMC speeds tends to promote an Early-Retroflection following *Ou and De Ruijter* (1986). Moreover, anticyclonic eddies from the Indian Ocean also induce an enhancement in EMC speeds and promotes an early eastward drift in the vicinity of ∼24.5°S. Figure S2 illustrates an example of anticyclonic eddies progression inducing an Early-Retroflection, and the shift from a Canonical-Retroflection to an Early-Retroflection case seen in Figure 4a. This also highlights how the presence of high EKE in Figure 4c may be associated with the arrival of anticyclonic eddies, as a cause of the Early-Retroflection, but not attributed as a consequence of an Early-Retroflection event.

A significant negative linear relationship, reaching -0.3 of correlation factor, is found between the EMC speed and EKE in Figure 4a at the West Madagascar area (blue box in Figure 4c). Figure 4f depicts the composite obtained for weaker EMC speeds (below one standard deviation) but with a more intense EKE in the Figure 4c blue box. The typical Canonical-Retroflection obtained reveals that this pattern is associated with a decrease in EMC surface speeds and the generation of eddies after separating from the coast (*Ridderinkhof et al.*, 2013). Based on *de Ruijter et al.* (2004) and *Ridderinkhof et al.* (2013), eddy dipoles, cyclonic inshore and anticyclonic offshore, are typical patterns of the southern EMC extension, explaining the higher EKE when EMC is in a Canonical-Retroflection mode.

The third pattern on Figure 4g is obtained from a composite associated with diminished EKE in both West and East Madagascar areas (blue and green boxes on Figures 4b and 4c). This corresponds to a No-Retroflection case. In this case, a straight flow towards the African continent is associated with a minimum in eddy generation. On the other hand, the EKE temporal composites (Figure 4b,c) are also consistent with the indicated locations for retroflection, in green and blue stars (Figure 4e,f), which show the presence of remarkable EKE at each attributed to retroflection location. The presence of EMC retroflections is associated with mesoscale eddies occurring in both locations of Early-Retroflection and Canonical-Retroflection areas, together with the modulation of EMC strength.

4 Discussion and Conclusions

Using a suite of cruise data measurements, in-situ data, and satellite observations, this study reveals for the first time "where" the EMC retroflection occurs. Three distinct types of retroflections are identified : Early-Retroflection, Canonical-Retroflection, and No-Retroflection. The classical view of a retroflection south of Madagascar, beyond the southern tip, is here defined as a Canonical-Retroflection. The new state, the EMC Early-Retroflection, corresponds to the current turning back offshore from the East coast of the island. A retroflection position detected close to the African coastline until further down in the AC system is described as No-Retroflection. During 1993 to 2017 time period, retroflection (Early or Canonical) occurs 47% of the time, of which 13% is attributed to the Early-Retroflection. These findings corroborate the results highlighted by *Siedler et al.* (2009) who revealed that almost 50% of the EMC southern extension water feeds the AC system, while ∼40% contributes to the SICC formation.

By linking the EMC strength and the eddy activities in the retroflection areas, our study also proposes to answer "how" the retroflection can be formed. The retroflection position is EMC strength dependent, i.e. anomalous EMC speed favours retroflection, with a significant eddy activity contribution. Early Retroflection occurrences are found to be linked with the EMC volume transport. An EMC intensification can promote Early-Retroflection occurrences in agreement with *Ou and De Ruijter* (1986). The arrival of

mesoscale anticyclonic eddies at the east coast also contributes to the intensification of the EMC speed via a transfer of momentum and induces a premature eastward shift resulting in an Early-Retroflection. Similar events of eddy-current interactions have been described upstream of the AC where entrainment of anticyclonic eddies increase the current velocity and shift the AC offshore (*Braby et al.*, 2016). A reduced EMC speed may favour the presence of anticyclonic standing eddy at the southern tip of Madagascar, before the formation of eddy dipoles (*de Ruijter et al.*, 2004), which promote the Canonical-Retroflection case. Weaker EKE East and West of Madagascar, without dependency of the EMC strength, promotes a No-Retroflection case with a continuous flow propagating from the EMC southern extension straight toward the AC without interruption.

The irregular arrival of Rossby waves and impinged eddies, originating from the Indian Ocean and congregating at 25°S (*Schouten et al.*, 2002,0; *de Ruijter et al.*, 2004; *Quartly et al.*, 2006; *Halo et al.*, 2014), induced difficulties in clearly identifying the original location of the EMC retroflection and the source of the SICC from VMADCP observations (Figure 1). The combination of altimetry with in-situ data reveals that anticyclonic eddies passing through 25°S are associated with the retroflection in addition to contribution of the EMC core strength. Since it was difficult to interpret the Early Retroflection as a retroflection in previous literature (*Lutjeharms*, 1988; *Quartly and Srokosz*, 2002), this study has devoted a significant part to show the evidences, as well as to describe the dynamical processes, and the impact of the early EMC eastward veering from the coast at 25°S on a monthly as well as daily time scales.

Identification of the different EMC retroflection patterns leads to the understanding of their influence on the South-East phytoplankton bloom, coastal upwelling, connection with SICC, as well as to the variability of AC retroflection. A spatially coherent structure is found between composites of Early-Retroflection circulation patterns and chlorophyll-a concentration, during the same period (Figure 3e). Moreover, Figure 5a reveals that the prevalence of phytoplankton bloom in summer as described by *Dilmahamod et al.* (2019) could be mainly associated with an EMC Early-Retroflection. Although this bloom generation is caused by multiple processes (*Dilmahamod et al.*, 2019), the Early-Retroflection could be a contributor for summer bloom occurrences. In addition, the composite of surface currents built from Early-Retroflection periods (Figure 5b) reveals that the EMC Early-Retroflection structure could act as a contributor of the SICC formation before its decomposition into three main jets offshore toward the east (*Menezes et al.*, 2016). This suggests that the transport of nutrient-rich water through the SICC from the east coast could induce a visible offshore chlorophyll-a concentration patch (Figure 3e, 5a). The retroflection structure allows an estimated lagged response with the South Madagascar coastal upwelling cell strength (*Ramanantsoa et al.*, 2018a)(Figure 5c). During an Early-Retroflection, coastal upwelling becomes instantaneously weak (for one month), i.e. upwelling cell surface temperature anomaly becomes warm, while the EMC speed increases and shift offshore due to eddy activity (Figure 3), in line with *Dilmahamod et al.* (2019).

As EMC waters and eddies affect the AC (*de Ruijter et al.*, 2004; *Penven et al.*, 2006), a test is made on the sensitivity of the Agulhas retroflection to the EMC retroflection state (Figure 5d). A slight eastward shift of 0.2° degree is observed in the AC retroflection position in respond to the EMC retroflection state but the AC system still remains stable. Hence, the probable increase of the EMC retroflection occurrences, due to the current climate change situation, should be carefully monitored.

Numerical modelling studies could be performed in future for a better understanding of the physical mechanisms associated with accelerated ocean current scenarii interacting with mesoscale eddies (anticyclonic and/or cyclonic) which may induce intensification of EMC retroflection.

Acknowledgments

The authors want to thank the NRF SARCHi chair on Ocean Atmosphere Modelling for the funding. The volume transport data was sampled within the context of the INATEX program funded by Netherlands rganization for Scientific Research (NWO), section Earth and Life Sciences (ALW), through its ZKO Grant 839.08.431. Data sets are available through the ZKO data portal (http ://data.zkonet.nl/). We thank Prof Martin Visbeck (GEOMAR) and Dr Raymond Roman (UCT) for providing some cruise data sets utilised in this study. The ocean dynamic topography data has been obtained from Copernicus Marine Environment Monitoring Service (CMEMS)(`http://marine.copernicus.eu/`). Global drifter data used in this study was collected from the National Oceanic and Atmospheric Administration (NOAA), Physical Oceanography Division (PhOD), Global Drifter Program (`https://www.aoml.noaa.gov/phod/gdp/index.php/`).

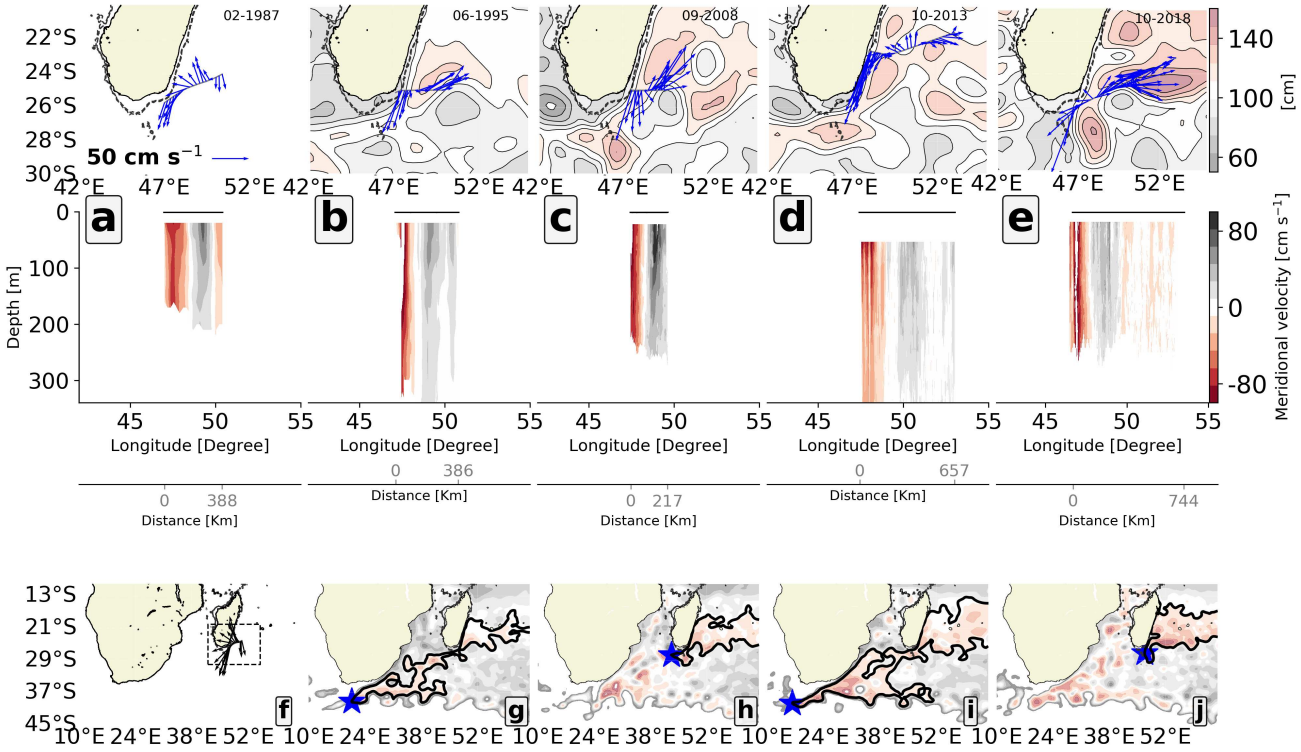

Figure 1. Hydrographic tracking of the EMC retroflection at ∼25°S. Panels (a) to (e) are transects showing the horizontal (top) and the vertical (bottom) structure of the EMC southern extension measured from VMADCP (Cruise data period and details are in the Supplementary Information Table S1). (top) Arrows represent directions and intensities of the near surface flow (∼20 m). Grey lines indicate the selected vessels trajectories. Overwritten maps represent weekly ADT according to each VMADCP measurement periods (bottom). Note that satellite altimetry data were not available during the 1987 cruise for the first panel (a). Vertical sections for each transect are presented along a longitude axis. Black horizontal lines at 0 m present the measured distance scale of each transect. Panels (g) to (j) illustrate the EMC retroflection position detection from sea level contours. Blue stars highlight the westernmost point of the contour, considered as the EMC retroflection position. Maps are the enlarged views of ADT maps seen in panel (a) to (e).

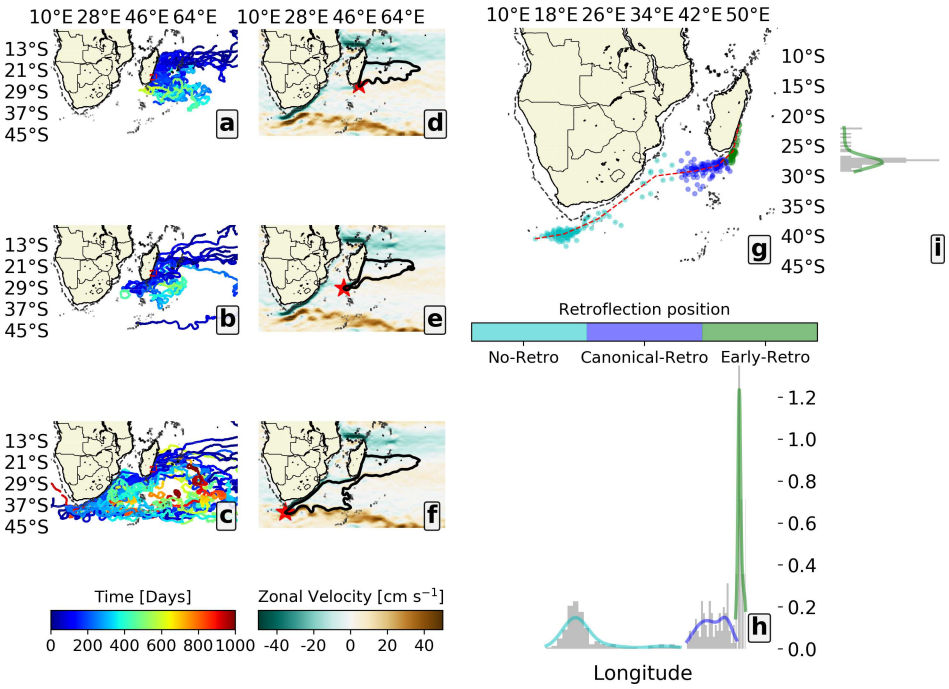

Figure 2. EMC retroflection spatial extent. Panels (a), (b) and (c) present trajectories and time durations of surface drifters floats depicting the three cases of EMC retroflection. (a) Selected surface drifters which follow the EMC Early-Retroflection case. (b) Drifters which depicts the EMC Canonical-Retroflection. (c) Combined drifters which represents the EMC No-Retroflection case. Panels (d), (e) and (f) display composites of detected EMC retroflection positions using the sea level height from satellite altimetry. The black contour represents the EMC and its retroflection. Red stars highlight the westernmost point of the selected sea level height contour, considered as the EMC retroflection position. Maps are composites of the zonal velocity corresponding to each retroflection cases. (g) presents the spatial classification of the EMC retroflection position from the unsupervised k-mean clustering. Each classified EMC retroflection case is used to build the composites of panels (d), (e) and (f). The dotted red line delineates the most probable location of EMC retroflection positions. (h) displays the longitudinal distributions of the 3 EMC retroflection cases. (i) displays the latitudinal distribution for the Early-Retroflection case.

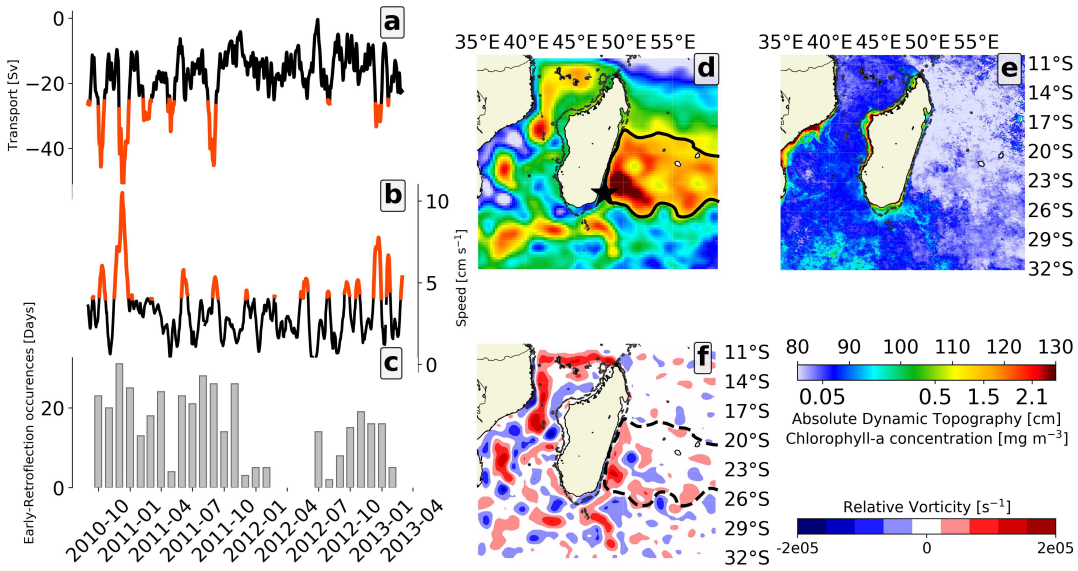

Figure 3. Evidence of the EMC Early-retroflection. (a) Time series of EMC northward volume transport computed from long-term measurement from ADCP (*Ponsoni et al.*, 2016). (b) Time series of the surface geostrophic currents computed from the sea level height from the satellite altimetry at the same location of the moored ADCP (∼23°S). EMC current speeds and volume transports higher than the standard deviation are highlighted in red. (c) Monthly EMC Early-Retroflection occurrences computed from the retroflection detection algorithm. (d) Composite of ADT for the periods of absolute EMC volume transports above the standard deviation (red lines in panel a). Black contour and star indicate the identified mean EMC Early-Retroflection extent. (e) and (f) Composites of Chlorophyll-a concentration (e) and relative vorticity (f) for the same Early-Retroflection periods.

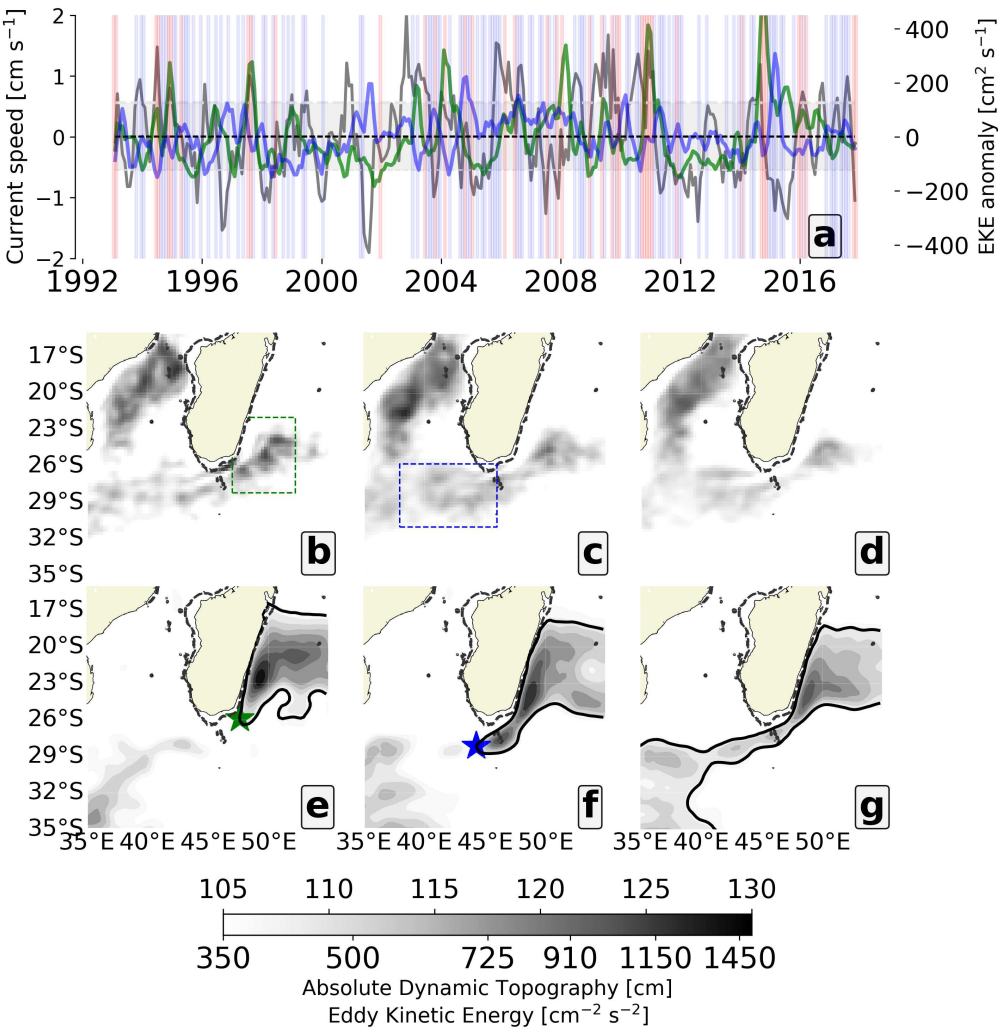

Figure 4. Dynamical processes associated with the EMC retroflection cases. (a) Grey time series presents the extended monthly EMC surface current speed anomalies from the satellite altimetry used in Figure 3b. Grey shaded area delimits the time series standard deviation. The green (blue) time series presents the EKE extracted from the green (blue) box in b (c). All signals are filtered using a three months running mean. Vertical bands colored in red indicate EMC Early-Retroflections, while blue bands indicate the detected EMC Canonical-Retroflections. (b), (c), and (d) are composite of EKE occurring during each retroflection case. (e) is the composite of the ADT when the EMC surface speeds and the EKE (green box in (b)) are abnormally higher, ie, above the positive standard deviation. (f) is the composite of the ADT corresponding with the period of weaker EMC surface speeds, below the standard deviation, but with high EKE (blue box in (c)). (g) is built from the composite of the period associated with weaker EKE for both green and blue boxes in (b) and (c). For (e) and (f) green and blue stars represent the EMC retroflection positions.

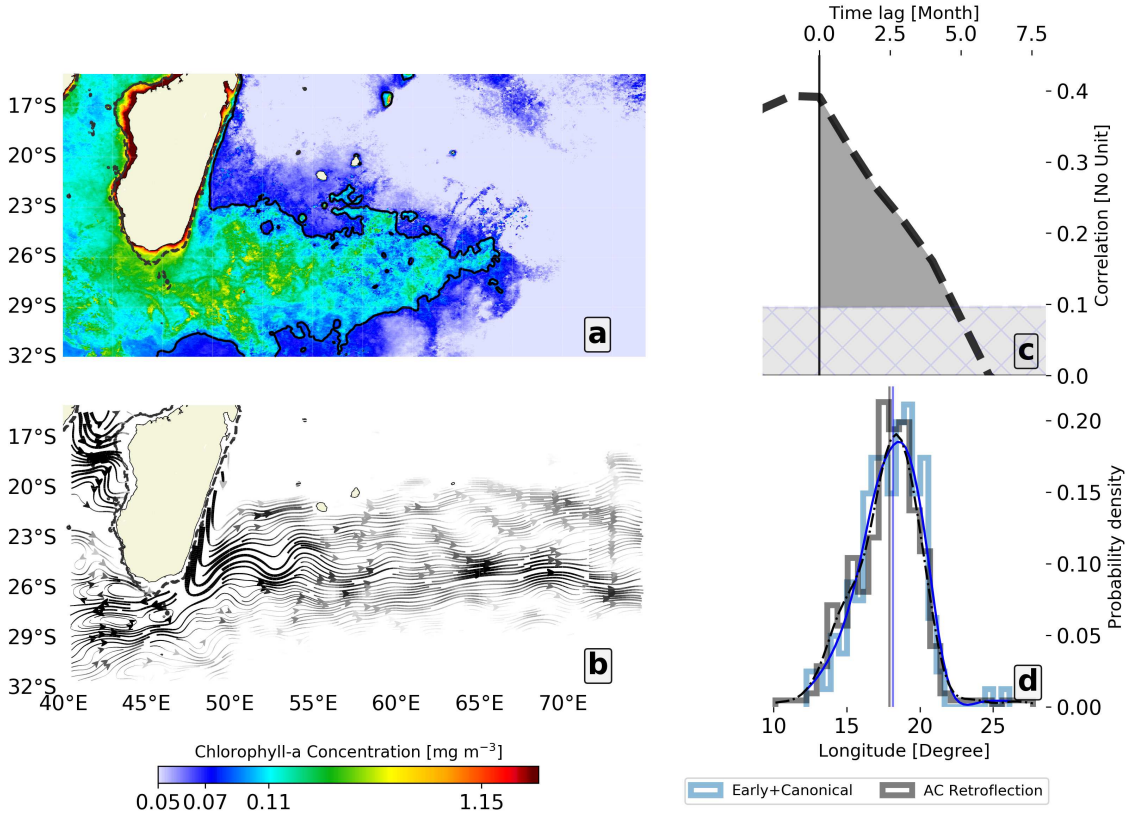

Figure 5. Local and regional impact of the EMC retroflections. (a) Composite of chlorophyll-a concentration during the periods of EMC Early-Retroflection occurrences in summer. Contour depicts the 0.07 mg m^{-3} chlorophyll-a concentration (*Dilmahamod et al.*, 2019). (b) Composite of surface current directions during the EMC Early-Retroflection periods. Only current speeds above 10 cm s^{-1} are shown. (c) Lag correlation between the longitudinal EMC retroflection positions and the coastal upwelling surface temperature anomalies (*Ramanantsoa et al.*, 2018a). (d) Comparison of statistical distribution of the longitudinal density between all the AC retroflection positions (grey), and the composite of the AC retroflection positions during EMC retroflection occurrence periods (EMC Early-Retroflection plus EMC Canonical-Retroflection periods)(blue shaded), with their respective Gaussian distributions.

Références

Backeberg, B. C., P. Penven, and M. Rouault (2012), Impact of intensified indian ocean winds on mesoscale variability in the agulhas system, *Nature Climate Change*, *2*(8), 608.

Bemiasa, J. (2009), Dynamique des pecheries traditionnelles d'anchois, de calmars et de poulpes du sud-ouest de Madagascar : utilisation d'outils oceanographiques pour la gestion des ressources., Ph.D. thesis, Universite de Toliara, Madagascar.

Braby, L., B. C. Backeberg, I. Ansorge, M. J. Roberts, M. Krug, and C. J. Reason (2016), Observed eddy dissipation in the agulhas current, *Geophysical Research Letters*, *43*(15), 8143–8150.

de Ruijter, W. P., H. M. van Aken, E. J. Beier, J. R. Lutjeharms, R. P. Matano, and M. W. Schouten (2004), Eddies and dipoles around South Madagascar : formation, pathways and large-scale impact, *Deep Sea Research Part I : Oceanographic Research Papers*, *51*(3), 383–400, 10.1016/j.dsr.2003.10.011.

Dilmahamod, A. F., P. Penven, B. Aguiar-González, C. Reason, and J. Hermes (2019), A new definition of the south-east madagascar bloom and analysis of its variability, *Journal of Geophysical Research : Oceans*, *124*(3), 1717–1735.

Halo, I., B. Backeberg, P. Penven, I. Ansorge, C. Reason, and J. Ullgren (2014), Eddy properties in the Mozambique Channel : A comparison between observations and two numerical ocean circulation models, *Deep Sea Research Part II : Topical Studies in Oceanography*, *100*, 38–53, 10.1016/j.dsr2.2013.10.015.

Longhurst, A. (2001), A major seasonal phytoplankton bloom in the Madagascar basin, *Deep Sea Research Part I : Oceanographic Research Papers*, *48*(11), 2413–2422, 10.1016/S0967-0637(01)00024-3.

Loveday, B. R., J. V. Durgadoo, C. J. Reason, A. Biastoch, and P. Penven (2014), Decoupling of the agulhas leakage from the agulhas current, *Journal of Physical Oceanography*, *44*(7), 1776–1797.

Lumpkin, R., and M. Pazos (2007), Measuring surface currents with surface velocity program drifters : the instrument, its data, and some recent results, *Lagrangian analysis and prediction of coastal and ocean dynamics*, pp. 39–67.

Lutjeharms, J. (1988), Remote sensing corroboration of retroflection of the east Madagascar current, *Deep Sea Research Part A. Oceanographic Research Papers*, *35*(12), 2045–2050.

Lutjeharms, J., N. Bang, and C. Duncan (1981), Characteristics of the currents east and south of Madagascar, *Deep Sea Research Part A. Oceanographic Research Papers*, *28*(9), 879–899.

Menezes, V. V., H. E. Phillips, M. L. Vianna, and N. L. Bindoff (2016), Interannual variability of the south indian countercurrent, *Journal of Geophysical Research : Oceans*, *121*(5), 3465–3487.

Nauw, J., H. Van Aken, J. Lutjeharms, and W. De Ruijter (2006), Intrathermocline eddies in the southern indian ocean, *Journal of Geophysical Research : Oceans*, *111*(C3).

Nauw, J., H. Van Aken, A. Webb, J. Lutjeharms, and W. De Ruijter (2008), Observations of the southern east madagascar current and undercurrent and countercurrent system, *Journal of Geophysical Research : Oceans*, *113*(C8).

Ou, H. W., and W. P. De Ruijter (1986), Separation of an inertial boundary current from a curved coastline, *Journal of Physical Oceanography*, *16*(2), 280–289.

Palastanga, V., P. Van Leeuwen, and W. De Ruijter (2006), A link between low-frequency mesoscale eddy variability around Madagascar and the large-scale Indian Ocean variability, *Journal of Geophysical Research : Oceans*, *111*(C9).

Penven, P., J. Lutjeharms, and P. Florenchie (2006), Madagascar : A pacemaker for the Agulhas Current system ?, *Geophysical Research Letters*, *33*(17).

Ponsoni, L., B. Aguiar-González, H. Ridderinkhof, and L. R. Maas (2016), The East Madagascar Current : Volume transport and variability based on long-term observations, *Journal of Physical Oceanography*, *46*(4), 1045–1065, 10.1175/JPO-D-15-0154.1.

Quartly, G. D., and M. A. Srokosz (2002), Satellite observations of the agulhas current system, *Philosophical Transactions of the Royal Society of London. Series A : Mathematical, Physical and Engineering Sciences*, *361*(1802), 51–56.

Quartly, G. D., J. J. Buck, M. A. Srokosz, and A. C. Coward (2006), Eddies around MadagascarâĂŤThe retroflection re-considered, *Journal of Marine Systems*, *63*(3), 115–129, j.jmarsys.2006.06.001.

Raj, R. P., B. N. Peter, and D. Pushpadas (2010), Oceanic and atmospheric influences on the variability of phytoplankton bloom in the southwestern Indian Ocean, *Journal of Marine Systems*, *82*(4), 217–229, 10.1016/j.jmarsys.2010.05.009.

Ramanantsoa, H. J. D. (2018b), Variability of coastal upwelling south of madagascar, Ph.D. thesis, University of Cape Town.

Ramanantsoa, J. D., M. Krug, P. Penven, M. Rouault, and J. Gula (2018a), Coastal upwelling south of Madagascar : Temporal and spatial variability, *Journal of Marine Systems*, *178*, 29–37.

Renault, L., J. C. McWilliams, and P. Penven (2017), Modulation of the agulhas current retroflection and leakage by oceanic current interaction with the atmosphere in coupled simulations, *Journal of Physical Oceanography*, *47*(8), 2077–2100.

Ridderinkhof, W., D. Le Bars, A. Heydt, and W. Ruijter (2013), Dipoles of the South East Madagascar Current, *Geophysical Research Letters*, *40*(3), 558–562.

Schouten, M. W., W. P. De Ruijter, and P. J. Van Leeuwen (2002), Upstream control of agulhas ring shedding, *Journal of Geophysical Research : Oceans*, *107*(C8), 23–1.

Schouten, M. W., W. P. de Ruijter, P. J. Van Leeuwen, and H. Ridderinkhof (2003), Eddies and variability in the mozambique channel, *Deep Sea Research Part II : Topical Studies in Oceanography*, *50*(12-13), 1987–2003.

Siedler, G., M. Rouault, and J. R. Lutjeharms (2006), Structure and origin of the subtropical south indian ocean countercurrent, *Geophysical Research Letters*, *33*(24).

Siedler, G., M. Rouault, A. Biastoch, B. Backeberg, C. J. Reason, and J. R. Lutjeharms (2009), Modes of the southern extension of the east Madagascar current, *Journal of Geophysical Research : Oceans*, *114*(C1), 10.1029/2008JC004921.

Figure 1.

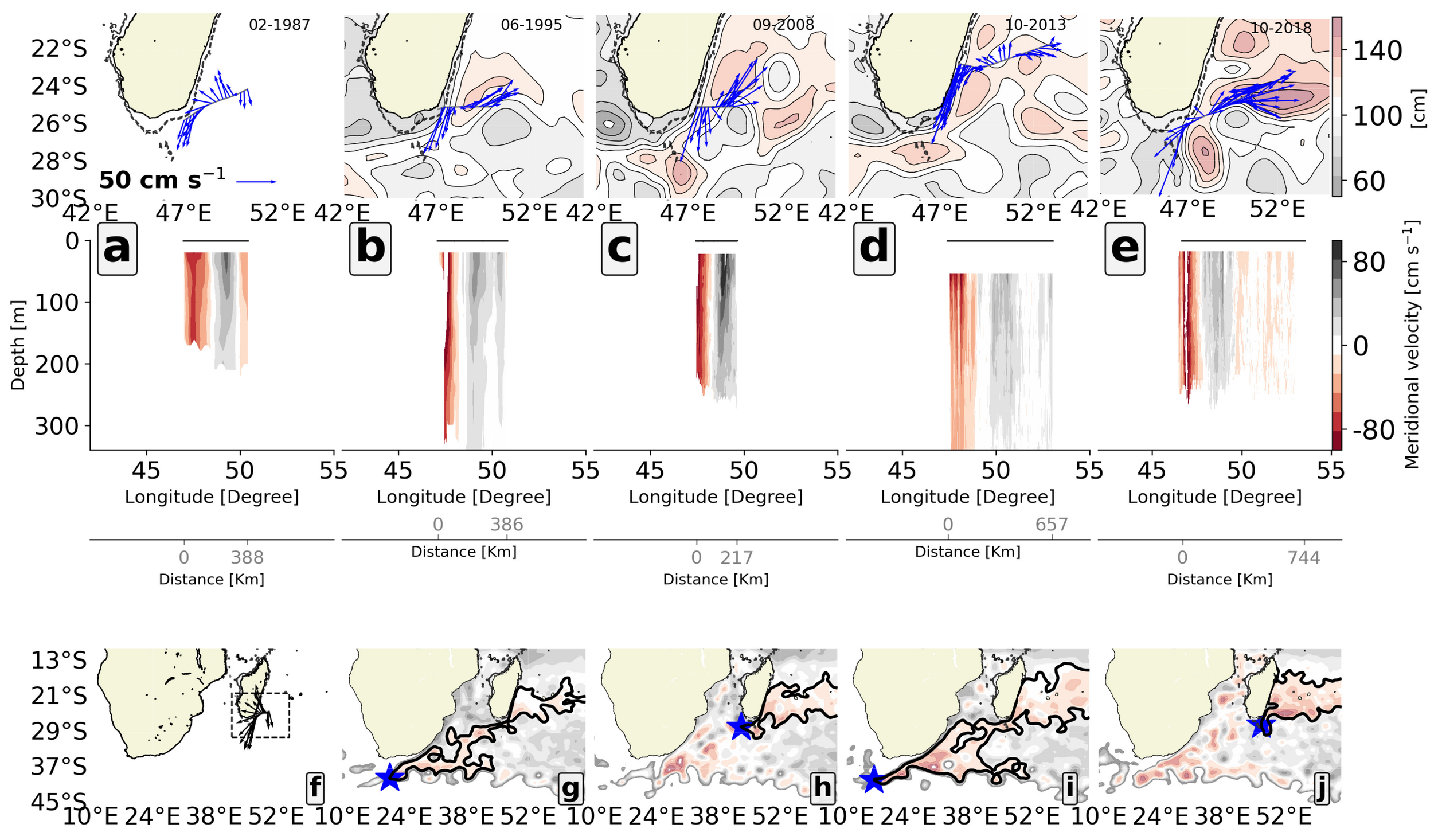
02-1987
06-1995
09-2008
10-2013
10-2018
50 cm s^{-1}
22°S
24°S
26°S
28°S
30°S
42°E
47°E
52°E
140
100
60
[cm]
a
b
c
d
e
Depth [m]
0
100
200
300
45
50
55
Longitude [Degree]
0
388
Distance [Km]
0
386
Distance [Km]
0
217
Distance [Km]
0
657
Distance [Km]
0
744
Distance [Km]
80
0
-80
Meridional velocity [cm s^{-1}]
13°S
21°S
29°S
37°S
45°S
10°E
24°E
38°E
52°E
f
g
h
i
j

Figure 2.

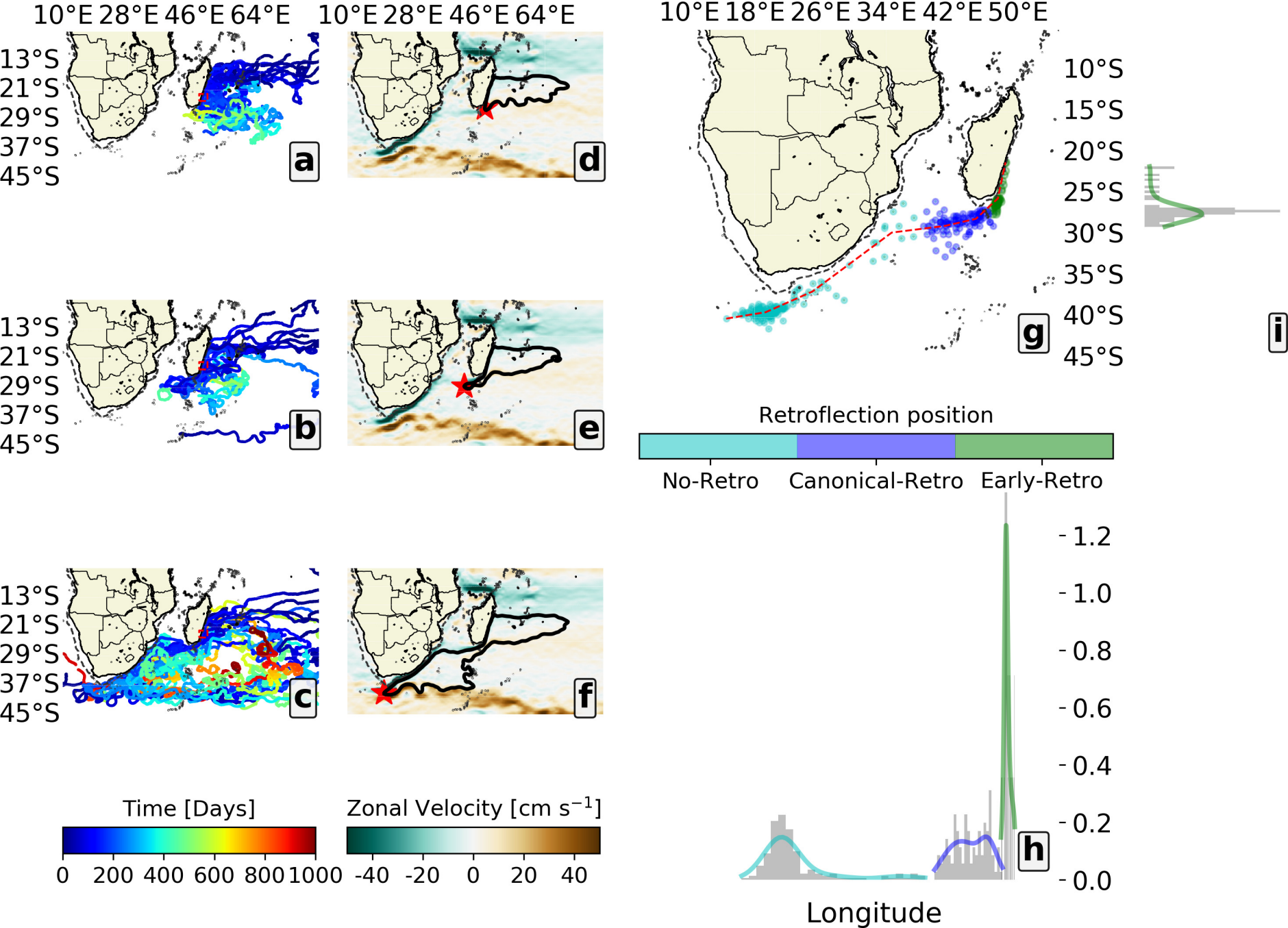
10°E 28°E 46°E 64°E
10°E 28°E 46°E 64°E
13°S
21°S
29°S
37°S
45°S
a
d
b
e
c
f
10°E 18°E 26°E 34°E 42°E 50°E
10°S
15°S
20°S
25°S
30°S
35°S
40°S
45°S
g
i
Retroflection position
No-Retro
Canonical-Retro
Early-Retro
1.2
1.0
0.8
0.6
0.4
0.2
0.0
h
Longitude
Time [Days]
0 200 400 600 800 1000
Zonal Velocity [cm s^{-1}]
-40 -20 0 20 40

Figure 3.

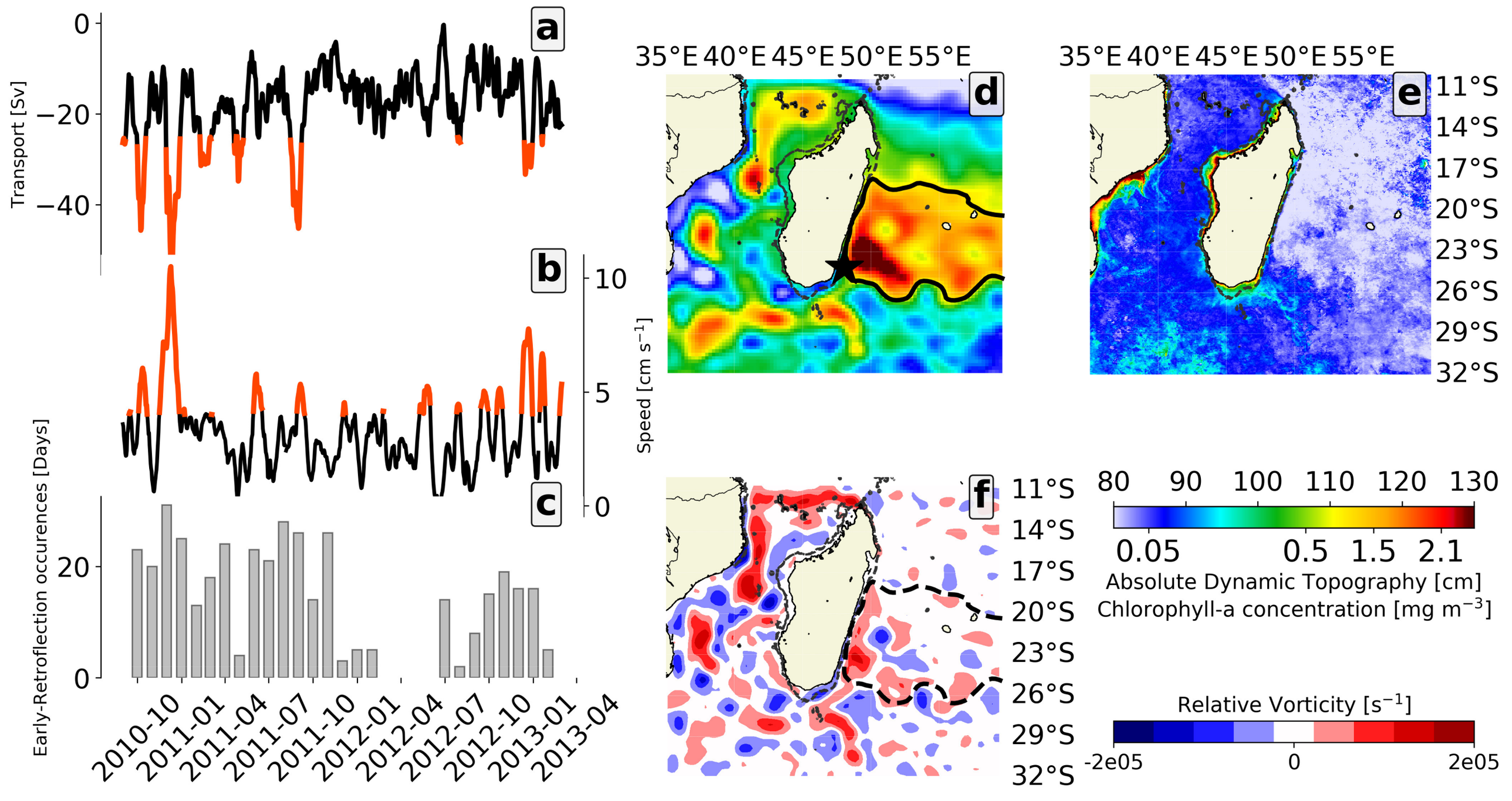
a
b
c
d
e
f
Transport [Sv]
0
−20
−40
10
5
0
Early-Retroflection occurences [Days]
20
0
2010-10
2011-01
2011-04
2011-07
2011-10
2012-01
2012-04
2012-07
2012-10
2013-01
2013-04
35°E 40°E 45°E 50°E 55°E
Speed [cm s^{-1}]
11°S
14°S
17°S
20°S
23°S
26°S
29°S
32°S
80 90 100 110 120 130
0.05 0.5 1.5 2.1
Absolute Dynamic Topography [cm]
Chlorophyll-a concentration [mg m^{-3}]
Relative Vorticity [s^{-1}]
-2e05 0 2e05

Figure 4.

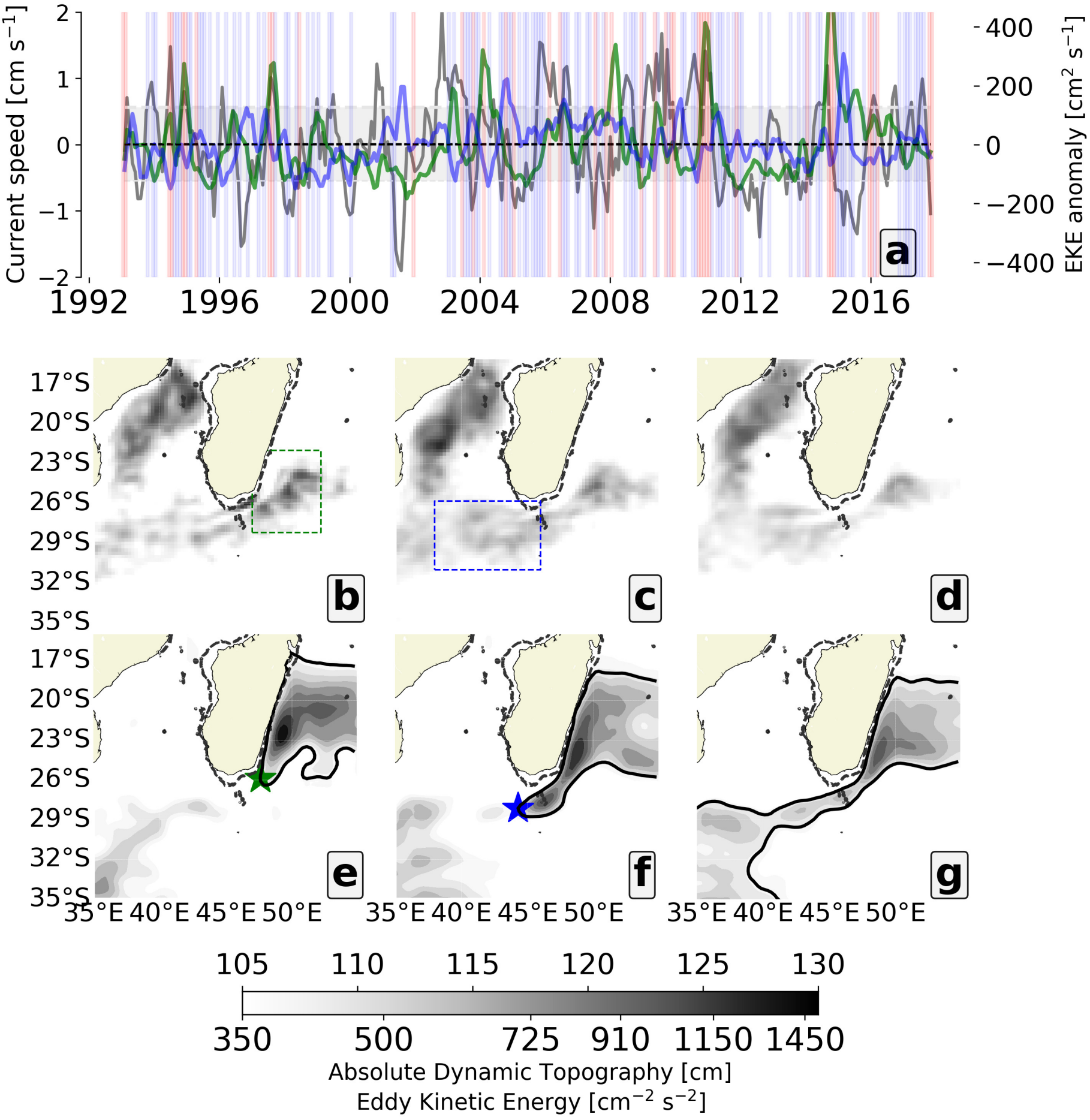
Current speed [cm s^{-1}]
EKE anomaly [cm^2 s^{-1}]
2
1
0
−1
−2
400
200
0
−200
−400
1992
1996
2000
2004
2008
2012
2016
a
17°S
20°S
23°S
26°S
29°S
32°S
35°S
b
c
d
e
f
g
35°E
40°E
45°E
50°E
105
110
115
120
125
130
350
500
725
910
1150
1450
Absolute Dynamic Topography [cm]
Eddy Kinetic Energy [cm^{-2} s^{-2}]

Figure 5.

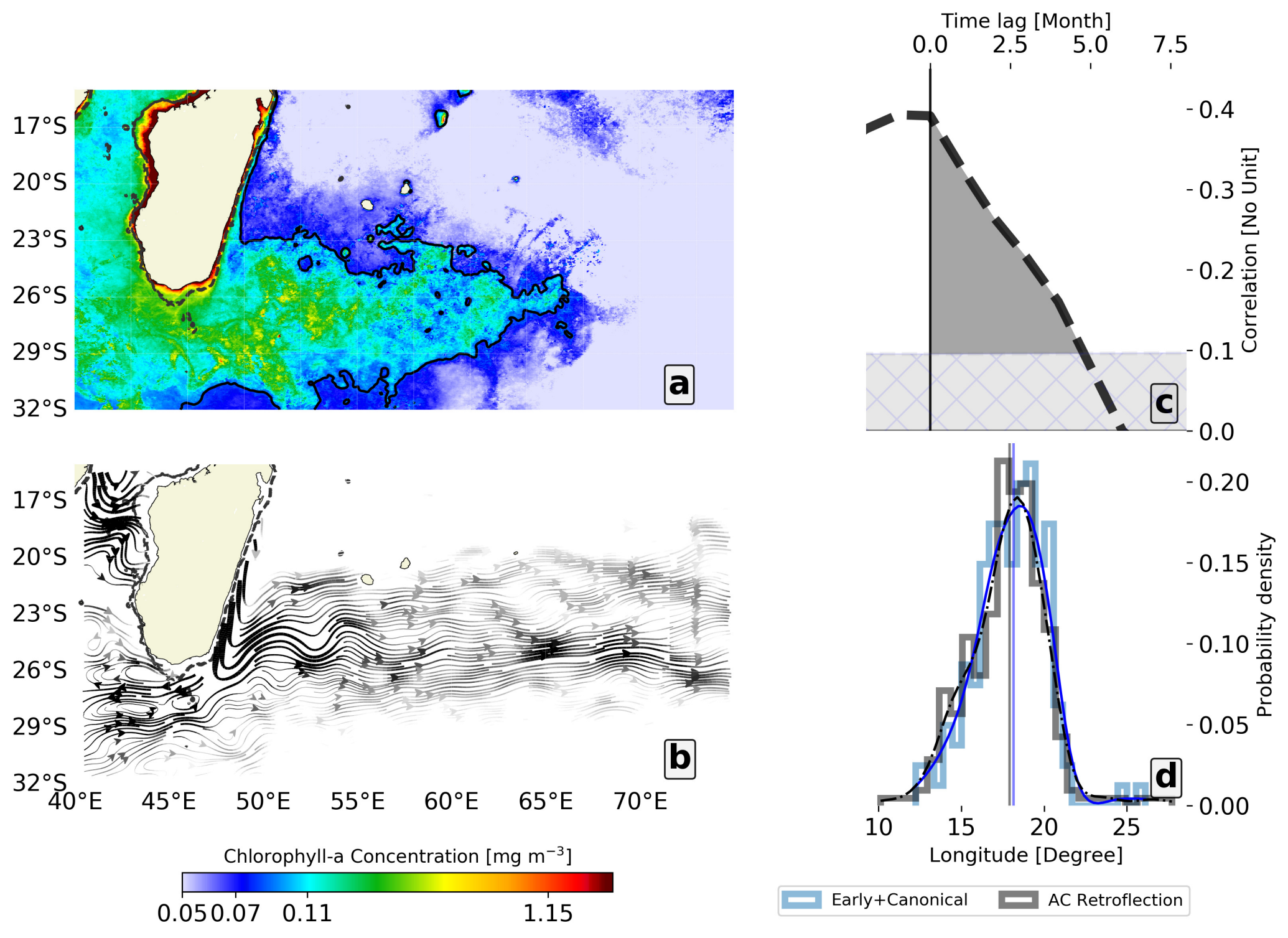
17°S
20°S
23°S
26°S
29°S
32°S
a
b
40°E
45°E
50°E
55°E
60°E
65°E
70°E
Chlorophyll-a Concentration [mg m^{-3}]
0.05
0.07
0.11
1.15
Time lag [Month]
0.0
2.5
5.0
7.5
0.4
0.3
0.2
0.1
0.0
Correlation [No Unit]
c
0.20
0.15
0.10
0.05
0.00
Probability density
d
10
15
20
25
Longitude [Degree]
Early+Canonical
AC Retroflection